Journal of Materials Chemistry C

ROYAL SOCIETY OF CHEMISTRY

PAPER

View Article Online
View Journal | View Issue

Check for updates

Cite this: J. Mater. Chem. C, 2024, 12, 11586

MXenes and polymeric colloids nanocomposites for EMI shielding

Edina Rusen, †*[a] Alexandra Mocanu,[ab] Oana Brincoveanu,[bc] Adina Boldeiu,[b] Cosmin Romanitan,[b] Martino Aldrigo,[b] Sergiu Iordănescu,[b] Aurel Diacon,[ad] Gabriela Toader†[d] and Raluca Gavrila[b]

Received 17th June 2024,
Accepted 27th June 2024

DOI: 10.1039/d4tc02519a

rsc.li/materials-c

This study presents the synthesis and characterization of nanocomposites based on polymer colloids (PC) and MXenes for applications in EMI shielding. The PCs were synthesized in the presence of MXenes by soap-free emulsion polymerization. The presence of the MXenes during the polymerization process induces changes in the nucleation process, which also occurs between the MXenes layers, leading to intercalated and finally fully exfoliated structures arising from the polymerization progress. Two co-monomer systems were synthesized in the presence of MXenes, both based on styrene (ST) and a second monomer, with different hydrophilic characteristics acrylic acid (AA) and hydroxypropyl methacrylate (HPMA), respectively. The nanocomposites were characterized by SEM, DLS, XRD, TGA, and EMI shielding capacity analyses. The analyses confirmed better compatibility between HPMA and the MXenes, which facilitated the formation of an exfoliated structure. The polymer colloids were incorporated into an epoxy resin to evaluate their EMI shielding abilities. The EMI tests showed that the electromagnetic properties of the epoxy film varied depending on the concentration of ST-HPMA-MXenes, resulting in increased electromagnetic transparency or absorption capacity.

Published on 04 July 2024. Downloaded on 7/19/2025 6:09:19 PM.

1. Introduction

Materials that exhibit transparency within specific frequency ranges are fundamental constituents in a wide array of aeronautical, space, and telecommunications applications.[1,2] The structures known as "radomes" are specifically shaped to shield antennas from a variety of atmospheric elements, such as rain, snow, dust, and heat. These enclosures effectively prevent damage while ensuring the optimal transmission and reception of high-frequency signals. For Internet of Things (IoT) applications,[3] which are the backbone of 5G and 6G communications,[3–5] small and lightweight protective systems are required to preserve miniaturized electronic components. The existing materials for radomes are not directly applicable to small IoT devices due to stringent requirements concerning dimensions and weight. Consequently, there is a genuine necessity to identify new electromagnetically transparent materials.

The X band (8.2–12.4 GHz) is a crucial electromagnetic frequency range with wide-ranging applications, including radar systems, terrestrial and space communications, traffic light motion sensors, and RF sources for particle accelerators. However, the prevalence of electromagnetic interference (EMI) in this band presents a significant challenge. As a result, extensive research has been conducted on various lightweight materials, such as conducting polymers, graphene, carbon nanotubes, and other nanocomposites, to explore their potential for EMI shielding purposes.[6] The ongoing advancement in electronic equipment miniaturization, in conjunction with the utilization of higher frequency ranges for 6G and/or 7G technologies, is projected to result in escalated power density. Consequently, this is anticipated to give rise to the production of substantial quantities of electromagnetic radiation.[7,8] Extended exposure to electromagnetic radiation can have significant effects on human health and negatively impact the functionality of other technological equipment.[9] The development of two-dimensional (2D) atomically thin structures has provided new materials for EMI shielding such as MXenes (*e.g.*, metal carbide and nitrides[10]), with performances similar to those of carbon-based nanomaterials.

The MXenes class encompasses a wide range of metal carbines and nitrides arranged in two-dimensional (2D)

[a] Faculty of Chemical Engineering and Biotechnologies, National University of Science and Technology Politehnica Bucharest, 1-7 Gh. Polizu Street, Bucharest, 011061, Romania. E-mail: edina_rusen@yahoo.com
[b] National Institute for Research and Development in Microtechnologies—IMT Bucharest, 126A Erou Iancu Nicolae Street, 077190 Bucharest, Romania
[c] Research Institute of the University of Bucharest, ICUB Bucharest, Soseaua Panduri, nr. 90, Sector 5, 050663, București, Romania
[d] Military Technical Academy, Ferdinand I", 39-49 G. Cosbuc Blvd., Bucharest, 050141, Romania
† Co-authors equally contributed to this study.

This journal is © The Royal Society of Chemistry 2024

Published on 04 July 2024. Downloaded on 7/19/2025 6:09:19 PM.

honeycomb lattices.[10] They are composed of several sheets of transition metal (M) with layers of carbon and/or nitrogen (X) atoms filling the octahedral sites between the adjacent transition metal layers.[11,12] The exceptional properties of MXenes have driven their widespread application across various fields. Notably, their electronic, magnetic, optical, electrochemical, and water barrier properties are highly esteemed for their practical utility.[13,14] MXenes display a unique combination of hydrophilicity and metallic conductivity due to free their surface functionalization and the free electrons of the transition metal carbide or nitride backbone.[15]

An appealing alternative solution for electromagnetic interference (EMI) shielding would consist of a coating formulation that allows facile deposition on diverse surfaces. Most coatings are polymer-based, consisting of polymer colloids with dimensions less than 1 μm dispersed in an aqueous media.[16,17] This consideration motivates the synthesis and characterization of a new nanomaterial based on polymer colloids and MXenes.

One of the most direct methods for obtaining polymer colloids of sub-micrometer dimensions is through the process of emulsion polymerization, with or without the inclusion of an emulsifier agent.[18,19] Soap-free emulsion polymerization[18,20] presents several advantages such as ease of purification, due to the absence of surfactant, improved mechanical and water-resistance properties of the resulting films,[21] high-solid content,[22] formation of stable colloidal particles (without the presence of a stabilizing agent). Achieving high monomer conversion and eliminating the use of surfactants not only renders the process more environmentally friendly but also streamlines the development of a diverse range of end products.

An innovative method for developing coatings with EMI shielding capabilities involves the production of polymer colloids through soap-free emulsion polymerization in the presence of MXenes. This approach leverages the advantages of photonic structures and MXenes-based materials. Our team has previously demonstrated the suitability of soap-free emulsion polymerization to afford polymer colloids capable of forming PCs by seeded polymerization using fullerene,[23,24] carbon nanotubes[25] and the possibility of using different hydrophilic co-monomers[26] and styrene as the main components. In this study, we opted for soap-free emulsion polymerization to ensure that the nucleation of particles in the formed micelles is not forced, thus allowing for the facilitation of particle nucleation between the MXene sheets. The MXenes 2D structures can be disrupted by simple introduction of –OH bearing molecules, such as polyvinyl alcohol,[27] between the sheets due to the hydrophilicity of the 2D MXenes.[28] The hydrophilicity of MXenes enhances their compatibility with hydrosoluble monomers when combined with styrene for the synthesis of polymer colloids and PC structures. This study is a pioneering experimental approach demonstrating the synthesis and characterization of polymer nanocomposites incorporating self-assembling submicron polymer colloids and MXenes. The synthesis and polymer nanocomposite formation stages are presented in Scheme 1.

2. Materials and methods

2.1. Materials

Styrene (ST) (Sigma-Aldrich), acrylic acid (AA) (Sigma-Aldrich), and hydroxy propyl methacrylate (HPMA) (Sigma-Aldrich) have been purified through vacuum distillation. Potassium persulfate ($K_2S_2O_8$) (KPS) (Merck) has been recrystallized from an ethanol/water mixture and then vacuum-dried. Nb_2AlC-MXenes (Sigma-Aldrich) was used as received. The utilized epoxy resin is comprised of two components: component A (the resin DER 332 (Aldrich)) and the amine component B (Jeffamine D400 (Aldrich)).

2.2. Methods

2.2.1. Synthesis of the polymer MXenes nanocomposites. Two samples (ST-AA-MXenes and ST-HPMA-MXenes) were obtained by soap-free aqueous emulsion polymerization. 1.3 mL of ST, 0.25 mL of AA or HPMA, and 0.1 g MXenes were added to 20 mL of distilled water with 13 mg of KPS. The polymerization reactions were nitrogen purged and then maintained for 4 h at 80 °C under continuous stirring at 350 rpm.

2.2.2. Synthesis of polymeric films based on MXenes. The final emulsions of ST-AA-MXenes and ST-HPMA-MXenes have been dialyzed for 7 days in distilled water using cellulose dialysis membranes (molecular weight cutoff, 12 000–14 000 Da), to remove the unreacted monomers and initiator. The water used for the dialysis procedure has been changed every 12 hours. The film was obtained by gravitational sedimentation on glass substrates and dried at 30 °C for 8 hours.

2.2.3. Synthesis of epoxy resin nanocomposites. 0.1 g ST-HPMA-MXenes or 0.2 g ST-HPMA-MXenes were dispersed in 10 g of component A of the resin, to which 5 g of component B was added. The mixture was kept at 80 °C for 24 hours to complete the reaction.

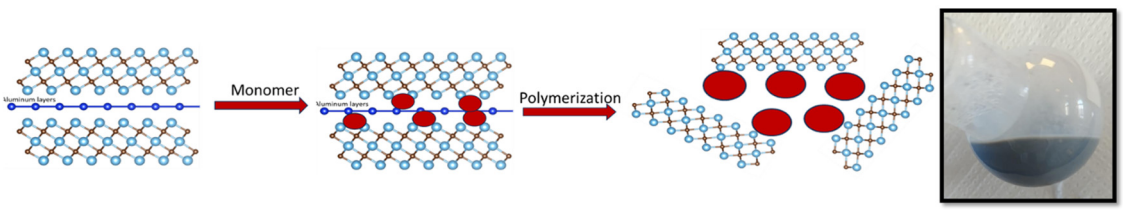

Scheme 1 The polymerization stages and the emulsion obtained in the presence of MXenes.

Published on 04 July 2024. Downloaded on 7/19/2025 6:09:19 PM.

2.3. Characterizations

The FT-IR analysis was performed on a Spectrum Two FT-IR spectrometer (PerkinElmer) equipped with a MIRacleTM single reflection ATR-PIKE Technologies at 4 cm^{-1} resolution, summing 16 scans in the 4000–400 cm^{-1} region.

The morphological and structural characterization of PDLC were acquired with a Nova NanoSEM 630 scanning electron microscope (FEI Company, Hillsboro, OR., USA) at an acceleration voltage of 10 kV and an element energy dispersive spectroscopy (EDX) system (Smart Insight AMETEK) at an acceleration voltage of 15 kV. The emulsions were deposited by vertical deposition on silica plates. To obtain high resolution of the micrograph images, the emulsions and the epoxy-based samples modified with colloids and MXenes were covered by a thin layer of Au (50 nm thickness).

Particle size measurements through dynamic light scattering (DLS) were performed in the water on a Nano ZS ZEN3600 Zetasizer (Malvern Instruments, Malvern, UK).

The thermogravimetric analyses (TGA) of the catalysts were performed using a Netzsch TG 209 F3 Tarsus equipment considering the following parameters: nitrogen atmosphere flow rate 20 mL min^{-1}; samples mass ~4 mg; temperature range: room temperature −900 °C; heating rate: 10 °C min^{-1} in an alumina (Al_2O_3) crucible.

X-ray diffraction (XRD) patterns were recorded using a 9 kW Rigaku SmartLab diffractometer (Osaka, Japan), equipped with a CuKα1 source that provides a monochromatic wavelength, λ = 0.15406 nm. During the measurements of the powder sample, the scan was initiated in $\theta/2\theta$ mode (*i.e.* the source and detector arms are coupled). For the other samples, on glass, a grazing-incidence XRD configuration was employed, for which the incidence angle of the source was kept constant at 0.5° to remove the signal from the glass substrate. In both configurations, the scan step was 0.01° min^{-1}, while the speed was set as 8° min^{-1}.

The measurements were performed with a Ntegra Aura system (Nt-MDT spectrum instruments) operated in semi-contact (Tapping) mode. A HA_NC (high accuracy noncontact AFM) probe with 3.5 N m^{-1} nominal force constant, 235 kHz resonant frequency and <10 nm nominal tip radius was employed for the measurements. To evaluate the film morphology and evenness, several areas of the exposed surface of the epoxy resin film containing the polymer colloids-Mxenes (ST-HPMA-MXenes 1) were scanned at sizes ranging from 25 to 40 μm. The acquired data were processed using the Nova software provided with the image analysis module, belonging to the Ntegra system.

In particular, the total EM shielding effectiveness (SE) is given by the following formula:

$$SE\ (dB) = SE_R\ (dB) + SE_A\ (dB) \quad (1)$$

in which SE_R is the shielding effectiveness related to EM reflections (R) and SE_A is the shielding effectiveness related to absorption (A) phenomena. In detail, we have:

$$SE\ (dB) = SE_R\ (dB) + SE_A\ (dB) = 10\log[(1 - |S_{11}|^2)^{-1}] + 10\log[(1 - |S_{11}|^2)/|S_{21}|^2] \quad (2)$$

Eqn (1) states that there are two fundamental physical mechanisms to modulate SE: (i) EM reflections (increased in the case of metals, which possess a high conductivity and a very low absorption); (ii) absorption due to dielectric losses and low conductivity (*e.g.*, as in graphene foams). SE cannot be reconfigured in the case of metals, while SE can be engineered in the case of composites by varying the concentration of their constituents.

The EMI shielding properties of the synthesized polymers (''RESIN'' for the non-functionalized sample, and ''ST-HPMA-MXenes 1'' and ''ST-HPMA-MXenes 2'' for the functionalized ones) has been measured with a calibrated VNA (vector network analyzer) connected to an X-band waveguide-based setup, as indicated in the lower left inset in Fig. 8. In detail, the scattering (S) parameters at the two ports have been measured providing the reflection and transmission coefficients at each port (S_{11} and S_{22} are the reflection parameters at the two ports, whereas S_{21} and S_{12} are the transmission parameters between the two ports). Using the measured S parameters, we can extract SE, SE_A, and SE_R which are represented in Fig. 8(a)–(c) for the three samples.

3. Results

The first stage of this study was to characterize the nanocomposite materials for differentiation between the two polymer matrixes and to ascertain the presence of the MAX signals specific to the unmodified MXenes.

Analyzing Fig. 1, it can be noted in the case of ST-AA-MXenes the presence of signals specific for the carboxyl group O–H stretch from 3300–2900 cm^{-1}, C=O stretch from 1760–1690 cm^{-1}, C–O stretch from 1320–1210 cm^{-1}, O–H bend from 1440–1395 and 950–910 cm^{-1}, respectively for the vibration specific for MAX phase at 550 cm^{-1}.[29,30] In the case of ST-HMPA, it can be observed that the signal at 3200–3550 cm^{-1} and respectively the vibrations of the inorganic phase are more intense compared to the

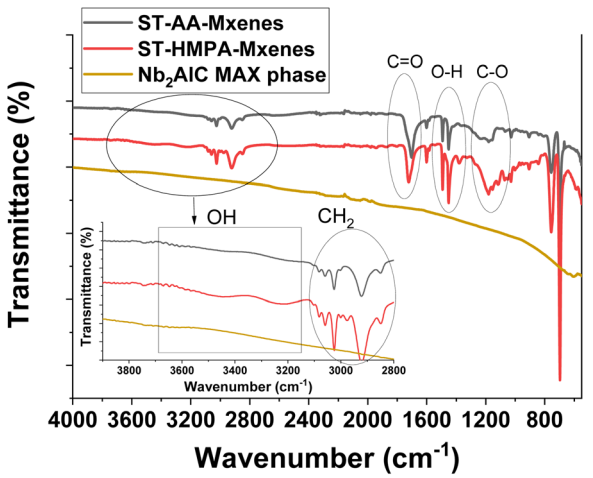

Fig. 1 FT-IR spectra of the ST-AA-MXenes, ST-HPMA-MXenes, and MAX phase.

 This journal is © The Royal Society of Chemistry 2024

Published on 04 July 2024. Downloaded on 7/19/2025 6:09:19 PM.

ST-AA-MXenes composite. It can be concluded that both materials contain polymeric and MXenes components.

The next step in the material characterization process involved examining the morphology using SEM. Thin films from the emulsions obtained in the presence of MXenes were analyzed using SEM.

From the analysis of Fig. 2a, it can be noted that the polymer colloids obtained partially cover the MXenes platelets, the polymer spheres adhering to the surface of the 2D structures forming and intercalated morphology. In the second case, illustrated in Fig. 2b, the presence of an exfoliated MXenes morphology is discernible, resulting in a distinct differentiation between two phases: the spherical polymer colloids and the exfoliated MXenes platelets. In order to validate these initial observations, DLS analysis was conducted to gain a more comprehensive understanding of the samples, given that SEM analysis provides insights into only a limited portion of the sample. Furthermore, an assessment of the Zeta potential values can serve to confirm the stability of the obtained latexes.

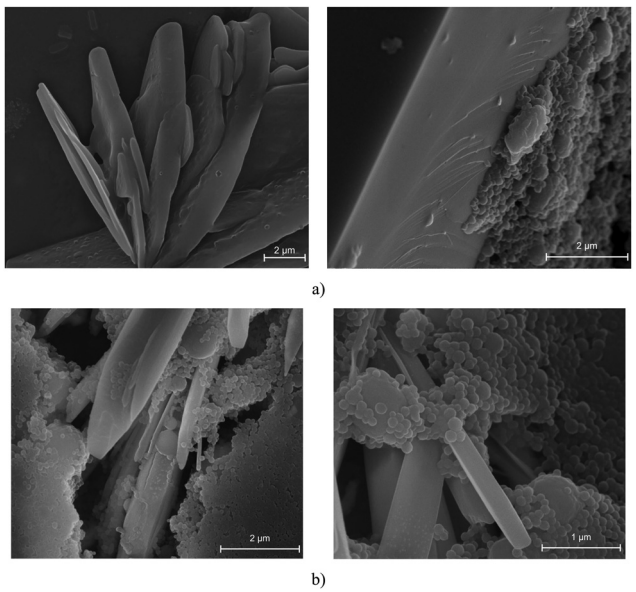

Fig. 2 SEM images of the samples: (a) ST-AA-MXenes and (b) ST-HPMA-MXenes.

In the case of the system ST-AA-MXenes (Fig. 3), the dimensions of the assembles formed were 1144 nm with a Zeta potential of −28.7 mV. Based on previous reports of our team,[26,31–34] for the ST-AA system, the polymer particle dimensions are in the 200–250 nm range for polymerization without MXenes. Thus, the DLS data presents the dimensions of the MXenes polymer colloid aggregates that were identified as polymer colloids bound to the 2D MXenes platelets. Also, the value of the Zeta potential indicates good stability of the polymer latex, while the negative sign is determined by the presence of the SO_4^{2-} resulting from the initiator utilized. In the case of the ST-HPMA-based system, the average dimension from the DLS analysis was 249 nm which corresponds to the hydrodynamic diameter of a polymer colloid. In addition, the Zeta potential value is much higher which indicates a higher stability of this latex. The dynamic light scattering (DLS) analysis reveals the presence of two distinct morphologies: an intercalated structure in the former case and an exfoliated configuration in the latter. This difference is ascribed to the compatibility between the MXenes and the water-soluble monomer units, namely AA or HMPA. Consequently, it can be inferred that owing to its hydroxyl groups, HMPA exhibits superior compatibility with the MXenes in contrast to the carboxyl groups present in acrylic acid.

To sustain the SEM and DLS analysis, the next investigation aimed to ascertain the crystalline characteristics of the obtained materials by XRD. The polymer-MXene films were analyzed *via* XRD. They were obtained by vertical deposition of the emulsions followed by drying to remove water. The results are presented in Fig. 4.

Analyzing Fig. 4, the diffraction pattern specific to the MAX phase Nb_2AlC can be observed, which is in accordance with the literature data.[35–37] Thus, for the modified MXenes, the peak

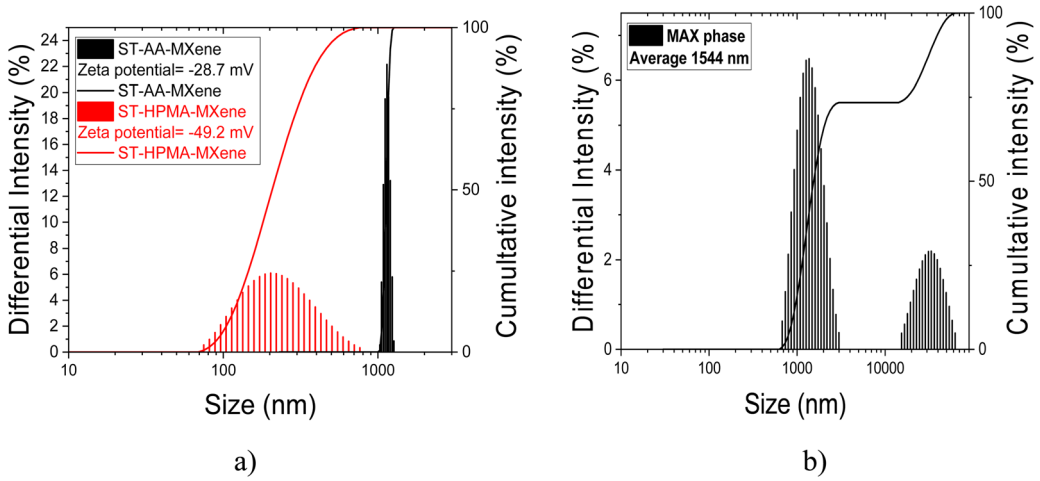

Fig. 3 DLS analysis for the (a) ST-AA-MXenes and ST-HPMA-MXenes and (b) pristine MXenes.

Published on 04 July 2024. Downloaded on 7/19/2025 6:09:19 PM.

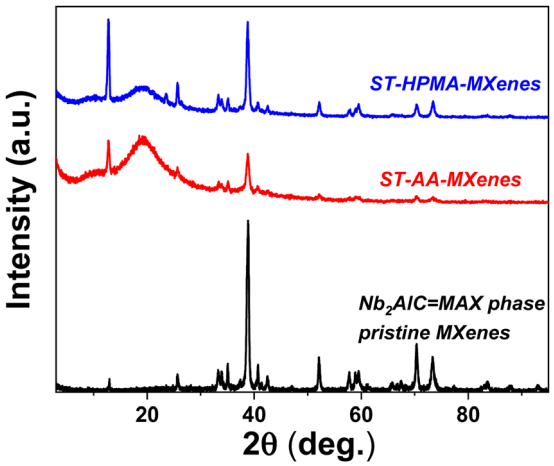

Fig. 4 XRD spectra for the ST-AA-MXenes, ST-HPMA-MXenes and Nb_2AlC–MAX phase of pristine MXenes.

centered at approximately 9.1° and 22.6° could be attributed to the characteristic peaks of $Nb_2C(002)$ and $Nb_2O_5(001)$, respectively,[38] and the presence of the characteristic peak at 9.1° confirmed that Nb_2C formed from Nb_2AlC. The XRD results appear to align with the morphologies identified in the SEM investigation and the DLS analysis. Comparing the two nanocomposites, it is evident that in the case of ST-HPMA-MXenes, the characteristic signal at 9.1° is more intense than for the ST-AA-MXenes. Thus, a more exfoliated structure can be attributed to ST-HPMA-MXenes colloids.

Thermal resistance is an important characteristic that requires careful consideration depending on specific applications. As such, the four specimens (ST-AA-MXenes, ST-HPMA-MXenes, and the polymer colloids without MXenes) were subjected to TGA analysis to determine the influence of the MXenes on the thermal resistance of the materials.

The analysis of TGA results (Fig. 5) reveals that the polymer decomposition occurs around 410 °C, resulting in different quantities of residual mass. Thus, in the case of ST-AA-MXenes, the residual mass is around 25% which can be attributed to a stable aggregate formed between MXenes and polymer. The existence of aggregates was also confirmed by DLS, XRD, and SEM analysis. Nevertheless, both MXenes-based composites display a slightly higher thermal resistance.

In applications such as EMI shielding, the polymeric layer (consisting of resin and filler) must be applied by brushing or spraying onto various surfaces. Thus, the nanocomposites were dispersed in an epoxide resin (component A) to which the reactive diamine component was added (component B). The hardening time was 24 hours which is sufficient to facilitate application and use. The nanocomposite ST-HPMA-MXenes was chosen for this step. Two different concentrations of ST-HPMA-MXenes (0.1 g and 0.2 g, respectively) were utilized in the final resin, resulting in varying concentrations of MXenes. After the hardening of the resin containing the nanocomposite,

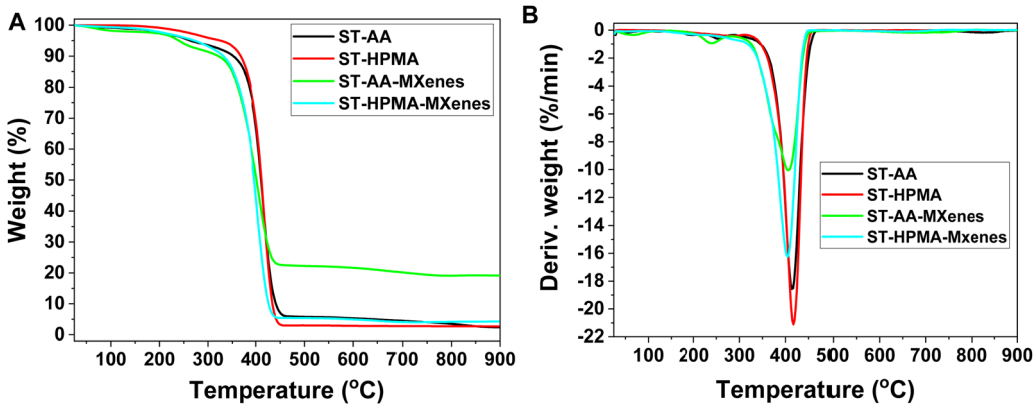

Fig. 5 TGA (A) and DTA (B) spectra for ST-AA, ST-HPMA, ST-AA-MXenes and ST-HPMA-MXenes.

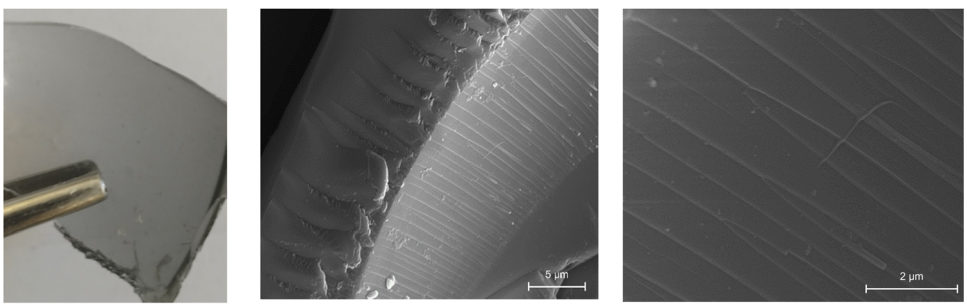

Fig. 6 Digital image and SEM analysis of epoxy resin film containing the polymer colloids-Mxenes (ST-HPMA-MXenes 1).

 This journal is © The Royal Society of Chemistry 2024

Published on 04 July 2024. Downloaded on 7/19/2025 6:09:19 PM.

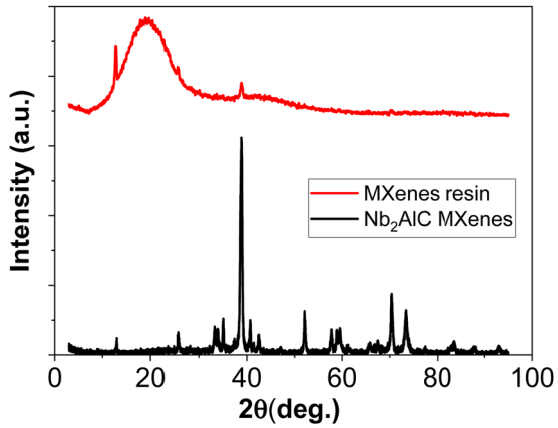

Fig. 7 XRD spectra for the MXenes resins and MAX phase of pristine MXenes.

SEM analysis was employed to investigate the obtained morphology (Fig. 6).

The obtained film displayed a grey color specific for MXenes, which sustains good compatibility between the MXenes, the polymer colloids, and the epoxy resin. The SEM images of the resin containing the polymer colloids – MXenes composites also confirm this good compatibility (Fig. 6).

For additional information, the obtained resin was characterized by XRD and compared with the MAX phase (pristine MXenes) in Fig. 7. From this analysis, it can be noticed the complete lack of signals specific for the MAX phase which sustains the obtaining of a fully exfoliated morphology that limits the formation of crystalline domains.

The AFM scans revealed a uniform and smooth surface of the film, without large deformations, featuring only small individual particles. The measured rms roughness was between 40 and 50 nm across all scanned areas, with a normal (Gaussian) distribution of the topography. This further supports the good compatibility of the MXenes, polymer colloids, and epoxy. A typical image of the film surface at 30 μm scan size is depicted in Fig. 8.

For the EMI shielding applications, from the experimental results, one can notice that SE_A is maximum for ST-HPMA-MXenes 2 but almost identical for RESIN and ST-HPMA-MXenes 1, whereas SE_R is maximum for ST-HPMA-MXenes 2 and minimum for ST-HPMA-MXenes 1. The relative permittivity ε_r of any material is a complex quantity $\varepsilon_r = \varepsilon' - j\varepsilon''$ and the imaginary part ε'' depends on the conductivity σ, the angular frequency ω, and the free-space permittivity ε_0, as follows: $\varepsilon'' = \sigma/\omega\varepsilon_0$. Also, the dielectric losses are expressed through the loss tangent $\tan\delta = \varepsilon''/\varepsilon'$. Hence, an increase in the absorption could come from an increase of the dielectric constant (ε'), an increase of $\tan\delta$, or a combination of the two (in this latter case, it means that ε'' also increases), whereas an increase of the EM reflections can be related to an increase of σ, hence to an increase of ε''. This seems the case for ST-HPMA-MXenes 2, which also exhibits the highest values for SE_R. Moreover, RESIN and ST-HPMA-MXenes 1 have almost identical values for SE_A, hence we can infer that they possess similar values of their relative permittivity.

As a whole, ST-HPMA-MXenes 2 offers a higher SE (Fig. 9(c)), meaning that it has the potential to be an EMI shielding material if one succeeds in further increasing its SE (*i.e.*, higher than 10–15 dB). On the contrary, ST-HPMA-MXenes 1 is better than RESIN as EM transparent material, likely due to a lower value of its dielectric constant, which reflects a lower absorption of the incident microwave signal.

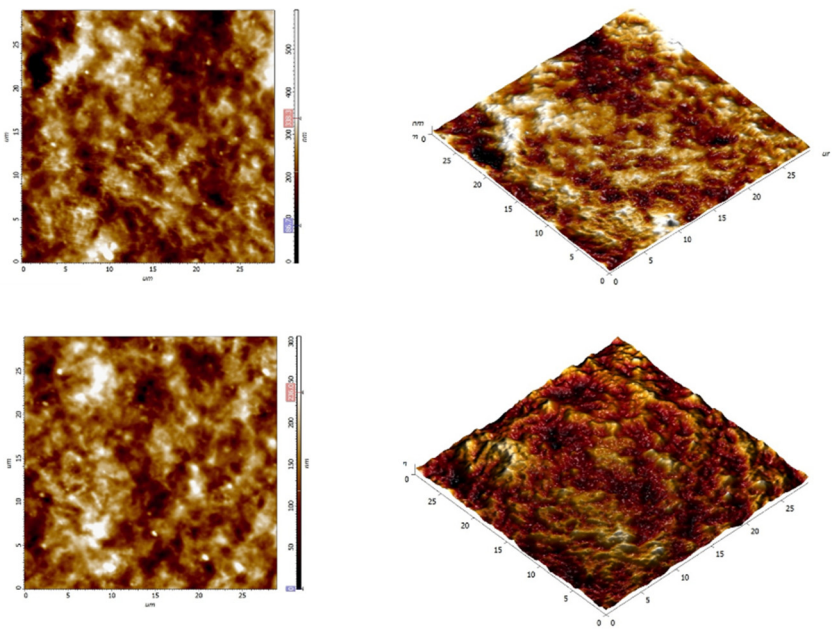

Fig. 8 AFM images for two different regions (depicted in the up and down rows) from the surface of the nanocomposite ST-HPMA-MXenes embedded in epoxy resin. Left: 2D scans. Right: 3D renderings.

Published on 04 July 2024. Downloaded on 7/19/2025 6:09:19 PM.

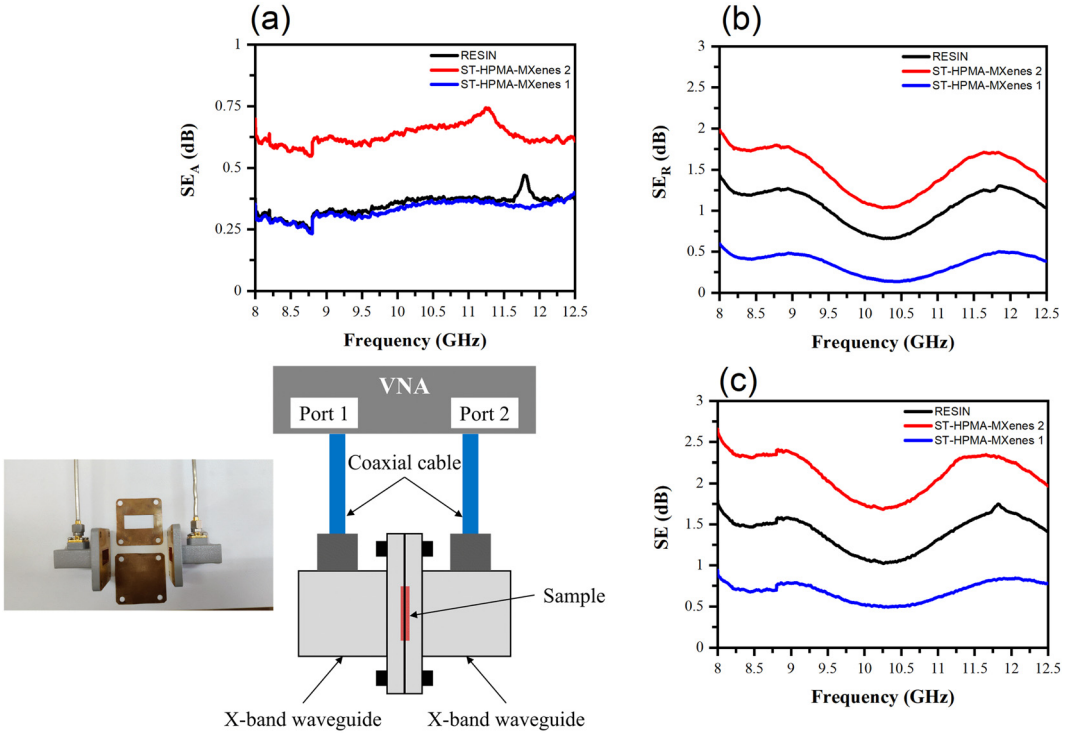

Fig. 9 Extracted (a) SE_A, (b) SE_A, and (c) SE for RESIN (solid black line), ST-HPMA-MXenes 2 (solid red line), and ST-HPMA-MXenes 1 (solid blue line) in the X band. Lower left inset: schematic of the microwave setup and picture of the X-band waveguides with some metallic parts used for the calibration.

4. Conclusions

This study presented the synthesis of new MXenes nanocomposites based on polymer colloids resulting from a soap-free emulsion polymerization performed in the presence of the MXenes. Two polymeric colloids were successfully synthesized: polystyrene-*co*-acrylic acid and polystyrene-*co*-hydroxypropyl methacrylate. The presence of MXenes during the polymerization process plays a crucial role in inducing the formation of intercalated and fully exfoliated structures. The final structure depends on the compatibility between the hydrophilic components. The FT-IR analysis confirmed the polymer formation and the presence of the MXenes. SEM analysis indicated an intercalated structure for ST-AA system while for ST-HPMA system a fully exfoliated structure was observed. This preliminary observation was confirmed by DLS, XRD, and TGA analyses.

The integration of polymer colloids-MXenes nanocomposites in an epoxy resin was utilized to assess the EMI characteristics. Significantly, the results demonstrate that, based on specific applications, it is feasible to engineer a material to provide electromagnetic transparency or EMI shielding properties through deliberate adjustment of MXenes concentration in the epoxy resin.

Data availability

The authors confirm that the data supporting the findings of this study are available within the article.

Conflicts of interest

There are no conflicts to declare.

Acknowledgements

This work was financially supported by the Ministry of Research, Innovation and Digitalization (UEFISCDI) through ctr.no. PTE80/2022 and ctr.no. 672PED/2022. M. A. would like to thank for financial support from Romanian Ministry of Research, Innovation and Digitization, through the Core Program within the National Research Development and Innovation Plan 2022-2027, under Project 2307.

References

1 G. S. Mani, in Radome Materials, ed. V. R. K. Murthy, S. Sundaram, B. Viswanathan, *Microwave Materials*, Springer Berlin Heidelberg, Berlin, Heidelberg, 1994; pp. 200–239.
2 N. Khatavkar and K. Balasubramanian, *RSC Adv.*, 2016, **6**(8), 6709–6718, DOI: **10.1039/C5RA18712E**.
3 Z. Qadir, K. N. Le, N. Saeed and H. S. Munawar, *ICT Express*, 2023, **9**(3), 296–312, DOI: **10.1016/j.icte.2022.06.006**.
4 D. Huang, Y. Chen, L. Zhang and X. Sheng, *J. Mater. Sci. Technol.*, 2023, **165**, 27–38, DOI: **10.1016/j.jmst.2023.05.013**.
5 M. C. Vu, P. J. Park, S.-R. Bae, S. Y. Kim, Y.-M. Kang, W. K. Choi, M. A. Islam, J. C. Won, M. Park and S.-R. Kim, *J. Mater. Chem. A*, 2021, **9**(13), 8527–8540, DOI: **10.1039/D0TA12306D**.

 This journal is © The Royal Society of Chemistry 2024

Published on 04 July 2024. Downloaded on 7/19/2025 6:09:19 PM.

6 S. Parveen and A. Manju, in Microwave Absorption and EMI Shielding Behavior of Nanocomposites Based on Intrinsically Conducting Polymers, Graphene and Carbon Nanotubes, ed. G. Ailton De Souza, *New Polymers for Special Applications*, IntechOpen, Rijeka, 2012, ch. 3.
7 Y.-J. Kwon, J.-B. Park, Y.-P. Jeon, J.-Y. Hong, H.-S. Park and J.-U. Lee, *Polymers*, 2021, **13**(8), 1312.
8 J. He, M. Han, K. Wen, C. Liu, W. Zhang, Y. Liu, X. Su, C. Zhang and C. Liang, *Compos. Sci. Technol.*, 2023, **231**, 109799, DOI: **10.1016/j.compscitech.2022.109799**.
9 R. Jaiswal, K. Agarwal, R. Kumar, R. Kumar, K. Mukhopadhyay and N. E. Prasad, *Soft Matter*, 2020, **16**(28), 6643–6653, DOI: **10.1039/D0SM00266F**.
10 F. Shahzad, M. Alhabeb, C. B. Hatter, B. Anasori, S. Man Hong, C. M. Koo and Y. Gogotsi, *Science*, 2016, **353**(6304), 1137–1140, DOI: **10.1126/science.aag2421**.
11 D. Ayodhya, *Diamond Relat. Mater.*, 2023, **132**, 109634, DOI: **10.1016/j.diamond.2022.109634**.
12 R. Akhter and S. S. Maktedar, *J. Materiomics*, 2023, **9**(6), 1196–1241, DOI: **10.1016/j.jmat.2023.08.011**.
13 M. S. Carey, M. Sokol, G. R. Palmese and M. W. Barsoum, *ACS Appl. Mater. Interfaces*, 2019, **11**(42), 39143–39149, DOI: **10.1021/acsami.9b11448**.
14 M. Carey, Z. Hinton, M. Sokol, N. J. Alvarez and M. W. Barsoum, *ACS Appl. Mater. Interfaces*, 2019, **11**(22), 20425–20436, DOI: **10.1021/acsami.9b05027**.
15 A. Kagalkar; S. Dharaskar and N. Chaudhari, 2D-Transition Metal Carbides and Nitrides: Prospects and Challenges, in *Age of MXenes, Volume 4. Applications in Advanced Catalysis and Membrane Processes*, ed. C. Nitin, American Chemical Society, 2023, vol. 1445, pp. 1–42.
16 F. M. Mwema and J. M. Wambua, Machining of Poly Methyl Methacrylate (PMMA) and Other Olymeric Materials: A Review, in *Handbook of Research on Advancements in the Processing, Characterization, and Application of Lightweight Materials*, ed. K. Kumar, B. S. Babu and J. P. Davim, IGI Global, Hershey, US, 1st edn, 2022, pp. 363–379, *(Advances in Chemical and Materials Engineering (ACME))*.
17 P. Zarras; M. D. Soucek and A. Tiwari, *Handbook of Waterborne Coatings*, Elsevier, 2020.
18 P. A. Lovell and F. J. Schork, *Biomacromolecules*, 2020, **21**(11), 4396–4441, DOI: **10.1021/acs.biomac.0c00769**.
19 C.-S. Chern, *Principles and applications of emulsion polymerization*, John Wiley & Sons, 2008.
20 C. G. Dobie and K. V. K. Boodhoo, *Chem. Eng. Process.*, 2010, **49**(9), 901–911, DOI: **10.1016/j.cep.2010.08.005**.
21 I. Martín-Fabiani, J. Lesage de la Haye, M. Schulz, Y. Liu, M. Lee, B. Duffy, F. D'Agosto, M. Lansalot and J. L. Keddie, *ACS Appl. Mater. Interfaces*, 2018, **10**(13), 11221–11232, DOI: **10.1021/acsami.8b01040**.
22 E. Bourgeat-Lami, T. R. Guimarães, A. M. C. Pereira, G. M. Alves, J. C. Moreira, J.-L. Putaux and A. M. dos Santos, *Macromol. Rapid Commun.*, 2010, **31**(21), 1874–1880, DOI: **10.1002/marc.201000305**.
23 E. Rusen, A. Mocanu, C. Corobea and B. Marculescu, *Colloids Surf., A*, 2010, **355**(1–3), 23–28, DOI: **10.1016/j.colsurfa.2009.11.020**.
24 E. Rusen, A. Mocanu and B. Marculescu, *Colloid Polym. Sci.*, 2010, **288**(7), 769–776, DOI: **10.1007/s00396-010-2197-7**.
25 A. Mocanu, E. Rusen, B. Marculescu and C. Cincu, *Colloid Polym. Sci.*, 2011, **289**(4), 387–394, DOI: **10.1007/s00396-011-2378-z**.
26 E. Rusen, A. Diacon and A. Mocanu, *Cent. Eur. J. Chem.*, 2014, **12**(1), 126–130, DOI: **10.2478/s11532-013-0356-7**.
27 S. Iravani and R. S. Varma, *Mater. Adv.*, 2023, **4**(19), 4317–4332, DOI: **10.1039/D3MA00365E**.
28 H. Guo, X. Wang, F. Pan, Y. Shi, H. Jiang, L. Cai, J. Cheng, X. Zhang, Y. Yang, L. Li, Z. Xiu, D. Batalu and W. Lu, *Nano Res.*, 2023, **16**(7), 10287–10325, DOI: **10.1007/s12274-023-5509-1**.
29 T. Yousaf, A. Areeb, M. Murtaza, A. Munir, Y. Khan and A. Waseem, *ACS Omega*, 2022, **7**(23), 19502–19512, DOI: **10.1021/acsomega.2c01143**.
30 J. Ji, L. Zhao, Y. Shen, S. Liu and Y. Zhang, *FlatChem*, 2019, **17**, 100128, DOI: **10.1016/j.flatc.2019.100128**.
31 E. Rusen, A. Mocanu, R. Somoghi, D. C. Culita, R. A. Mitran, A. Dinescu, A. Matei and A. Diacon, *Colloids Surf., A*, 2021, **614**, 11, DOI: **10.1016/j.colsurfa.2021.126158**.
32 E. Rusen, A. Diacon, R. A. Mitran, A. Dinescu, C. Nistor, R. Somoghi, A. C. Boscornea and D. Manaila-Maximean, *Eur. Polym. J.*, 2022, **175**, 8, DOI: **10.1016/j.eurpolymj.2022.111374**.
33 A. Diacon, E. Rusen, A. Mocanu, P. Hudhomme and C. Cincu, *Langmuir*, 2011, **27**(12), 7464–7470, DOI: **10.1021/la200878b**.
34 A. Diacon, E. Rusen, A. Mocanu and L. C. Nistor, *J. Mater. Chem. C*, 2013, **1**(28), 4350–4357, DOI: **10.1039/c3tc30172a**.
35 T. H. Scabarozi, J. Roche, A. Rosenfeld, S. H. Lim, L. Salamanca-Riba, G. Yong, I. Takeuchi, M. W. Barsoum, J. D. Hettinger and S. E. Lofland, *Thin Solid Films*, 2009, **517**(9), 2920–2923, DOI: **10.1016/j.tsf.2008.12.047**.
36 Z. U. Din Babar, J. Fatheema, N. Arif, M. S. Anwar, S. Gul, M. Iqbal and S. Rizwan, *RSC Adv.*, 2020, **10**(43), 25669–25678, DOI: **10.1039/D0RA04568C**.
37 H. Jin, K. Wang, Z. Mao, L. Tang and J. Zhang, *Adv. Electron. Mater.*, 2023, **9**(4), 2201071, DOI: **10.1002/aelm.202201071**.
38 H. Cheng and W. Zhao, *Friction*, 2022, **10**(3), 398–410, DOI: **10.1007/s40544-020-0469-x**.